How to cite: *Angew. Chem. Int. Ed.* **2024**, *63*, e202413758
doi.org/10.1002/anie.202413758

Hypervalent Compounds

The Trifluorooxygenate Anion $[OF_3]^-$: Spectroscopic Evidence for a Binary, Hypervalent Oxygen Species

*Deniz F. Meyer, Robert Medel, and Sebastian Riedel**

Dedicated to Professor Martin Jansen on the occasion of his 80th birthday

Abstract: Experimental evidence for hypervalent compounds of second-row elements is still scarce in literature. Here, we present the first report of the long-sought binary, hypervalent trifluorooxygenate anion $[OF_3]^-$. It was isolated in solid Ne matrices under cryogenic conditions after reacting oxygen difluoride with free fluoride ions from laser ablation of alkali metal fluorides MF (M = Li–Cs). VSEPR theory and calculations at the CCSD(T) level predict a C_{2v}-symmetric T-shape structure with one short and two long O–F bond lengths in $[OF_3]^-$. This is confirmed experimentally by FTIR spectroscopy in combination with isotopic labeling. Analysis of the natural local molecular orbitals shows the presence of one 2c–2e and one 3c–4e bond each. Natural resonance theory indicates the importance of the stability of $[OF_2]^{\bullet-}$ for the stability of $[OF_3]^-$. Although free $[OF_2]^{\bullet-}$ was not detected, the species MOF_2 (M = Na–Cs) could be observed in the same experiments, which are best described as contact ion pairs of $M^+[OF_2]^{\bullet-}$.

Lewis' concept of 2c–2e bonds and the octet rule by Langmuir have been very successful in explaining the bonding in many main group molecules.[1] However, hypervalent compounds violate these simple concepts and thus have been of great interest to chemists. The proponents of the Lewis model tried to explain this discrepancy with d orbital participation of the central atom, whereas ionic bonding was the favored picture held by people who saw the octet rule as more fundamental.[1a,2] Nowadays, mostly the Rundle-Pimentel model is used to describe these bonds as 3c–4e interaction of the p_σ orbitals, where one non-bonding electron pair is distributed over the terminal atoms.[3] This retains the octet rule for the central atom while setting it apart from purely ionic bonds. Throughout this work we refer to species as hypervalent if they feature 3c–4e interactions, as it was recently suggested.[4] This nomenclature does *not* imply an extension of the octet rule for the atom in question.

While this model captures the essence of hypervalent bonds, it predicts certain molecules to be stable, which are known to be transition states.[5] It was therefore refined in newer studies to address this issue. Molecular orbital (MO) theory approaches emphasize the slightly antibonding character of the "non-bonding" MO, due to the admixture of s orbitals, and the destabilizing effect of the p_π orbitals.[5a] However, bonding analyses based on valence bond (VB) calculations come to different conclusions. The recoupled-pair bonding formalism explains hypervalent bonds in terms of consecutive additions of radicals to a lone pair of the central atom. Here, the strength of the initially formed 2c–3e bond is seen as the important factor for the stability of the resulting species.[6] A similar picture was drawn for $[F_3]^-$, where the stability of $[F_2]^{\bullet-}$ has been shown to play a crucial role.[7]

Hypervalent compounds are typically formed by third- or higher row elements of the groups 13–18 in combination with highly electronegative bonding partners. The former prerequisite is still often seen as mandatory because only a few examples exist in which a second-row element may be considered as hypervalent, e.g., $[NO_3]^-$, O_3 and $[F_3]^-$.[6a,8] The lack of stable hypervalent second-row compounds has been attributed to their small size, leading to increased steric repulsion in the coordination sphere, and high ionization energies, which inhibits charge accumulation on the terminal atoms.[4,9] Indeed, a systematic computational study of 28 neutral and charged second-row element fluorides at the CCSD(T)/aug-cc-pVTZ level found only $[F_3]^-$ and $[OF_3]^-$ to be hypervalent and stable to dissociation.[4] The $[F_3]^-$ ion has been experimentally observed in matrix isolation[10] and in the gas phase[11] and exhaustively studied computationally.[12] In contrast, $[OF_3]^-$ is only predicted to be stable and all experimental attempts to prepare this species have failed so far.[4,13] While $[OF_3]^-$ was computed at the MP2/6-311+G(3df) level to be trigonal planar with three equivalent O–F bonds (D_{3h} symmetry),[13a] the calculations at the MP2(full)/6-311+G* and CCSD(T)/aug-cc-pVTZ level instead show a T-shape structure with two long and one short O–F bond (C_{2v} symmetry).[4,13b,c] The latter geometry is more consistent with the prediction of the valence shell electron pair repulsion (VSEPR) model, in which two lone pairs are

[*] D. F. Meyer, Dr. R. Medel, Prof. Dr. S. Riedel
Freie Universität Berlin, Fachbereich Biologie, Chemie, Pharmazie
Institut für Chemie und Biochemie—Anorganische Chemie
Fabeckstr. 34/36, 14195 Berlin
E-mail: s.riedel@fu-berlin.de

expected to occupy equatorial positions of a trigonal bipyramid (Figure 1).[4,13c]

Our goal was to synthesize $[OF_3]^-$ and determine its structure by means of FTIR spectroscopy. From previous matrix isolation experiments in our group we knew that free fluoride ions are formed in the plasma of laser-ablated alkali metal fluorides (MF),[10a] we therefore envisioned the synthesis of $[OF_3]^-$ by co-deposition of F^- with OF_2 in noble gas matrices. The formation energy of the T-shaped $[OF_3]^-$ is calculated to be $\Delta E_0 = -71.8$ kJ/mol at the CCSD(T)/aug-cc-pVTZ level, only moderately lower than for the formation of $[F_3]^-$ from F_2 and F^- (−96.2 kJ/mol). Computationally, we also located a second isomer, $[FOFF]^-$, which shows the presence of an F–F bond. However, this isomer is less stable by 41.5 kJ/mol relative to the T-shaped global minimum structure, details are provided in Figure S1 and Tables S1 and S2 in the Supporting Information. The electrostatic potential of OF_2 helps to rationalize this energetic order: due to the polarization of the bonds, the σ hole is more pronounced at the oxygen atom than at the more electronegative fluorine atoms (Figure 2). Also, in $[OF_3]^-$ the least electronegative atom is placed in the center of the 3c–4e bond, which was shown to be the most favourable arrangement for the valence isoelectronic interhalide anions.[14]

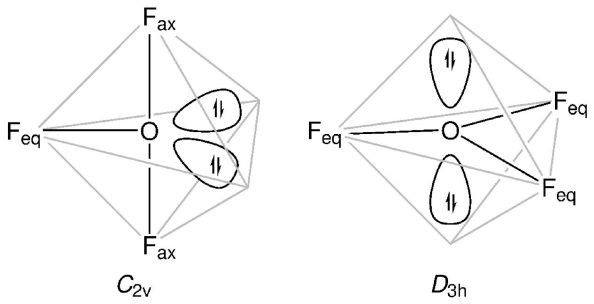

Figure 1. Possible structural arrangements of $[OF_3]^-$, with the fluorine atoms and lone pairs pointing towards the vertices of a trigonal bipyramid. VSEPR theory predicts the C_{2v} symmetric structure to be more favourable.

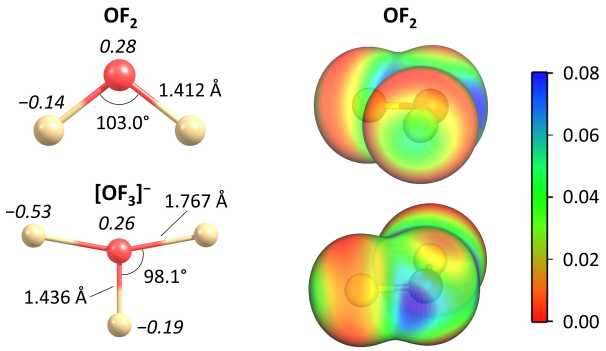

Figure 2. Left: Minimum structures of OF_2 and $[OF_3]^-$ (CCSD(T)/aug-cc-pVTZ). Oxygen atoms are depicted in red, fluorine atoms in beige. Italic values are the AIM charges calculated at the B3LYP-D3/aug-cc-pVTZ level. Right: Electrostatic potential of OF_2 mapped onto the electron density isosurface (0.01 a.u.). The potential values are given in a.u. View along one O–F bond onto F (top) and O (bottom).

The experiments were conducted by depositing a 1:1000 OF_2:Ne mixture onto a gold-coated copper mirror cooled to 5 K by a closed-loop helium cryostat. During the deposition, an alkali metal fluoride MF (M = Li–Cs) target was ablated inside the high-vacuum chamber by a pulsed Nd:YAG laser (1064 nm). Compared to the spectra of OF_2 and MF deposited separately, an additional band was present at 476.6 cm^{-1}, common for all alkali metal fluorides (Figures 3 and S2). It is assigned to the antisymmetric F_{ax}-O-F_{ax} stretching vibration of T-shaped $[OF_3]^-$ (Table 1). The intensity of the band decreased with the size of the metal ion and was barely visible for the smallest Na^+ and Li^+ cations (Figure S3), reflecting their increased interaction strength with the hard F^- anion according to the hard and soft acids and bases (HSAB) theory.[15] The low abundance of $[OF_3]^-$ is likely due to F^- binding more strongly to $F^\bullet$ and F_2 ($\Delta E_0 = -118.9$ and −96.2 kJ/mol, respectively) which are formed in the plasma by OF_2 homolysis, as evident from the detection of $^\bullet OF$ and $[F_3]^-$ (Figure S4).

After irradiation with a 470 nm LED the 476.6 cm^{-1} band was reduced in intensity, indicating that $[OF_3]^-$ is decomposed by light of this wavelength (Figure 3). Interestingly, even after prolonged irradiation a minor band remained. Subsequent irradiation with either 455 or 405 nm did not further photolyze the product, but 365 nm did. Nonetheless, full decomposition was only achieved after irradiation with 275 nm (Figures S5 and S6). A detailed analysis of the photochemistry of $[OF_3]^-$ is given in the Supporting Information (Tables S3 and S4, and text in Section S4).

Substituting $^{16}OF_2$ with $^{18}OF_2$ redshifted the 476.6 cm^{-1} band by 18.7 cm^{-1}, which is in good agreement with the calculated values for the assigned fundamental (Table 1).

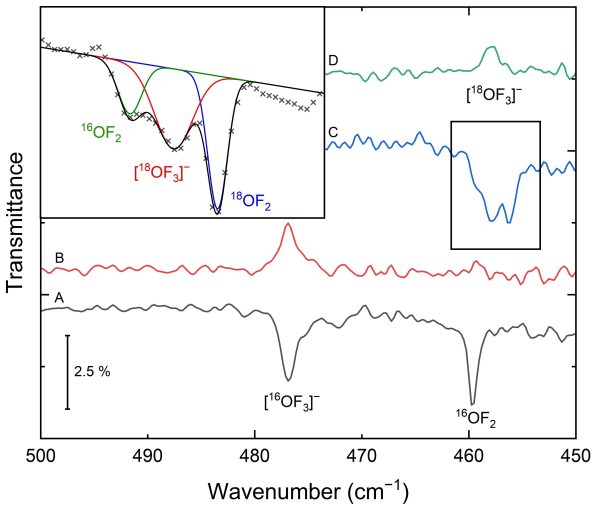

Figure 3. IR spectra of the reaction products after co-deposition of 0.1 % OF_2 in Ne with laser-ablated CsF for 120 min before and after subsequent irradiation. Spectra B and D are difference spectra. A: Before irradiation. B: After irradiation with 470 nm for 10 min. C: Same experiment as A using $^{18}OF_2$. D: After irradiation with 470 nm for 10 min. The inset shows the deconvolution of the spectral region around the $\delta(^{16}OF_2)$, $\delta(^{18}OF_2)$ and $\nu_{as}(F_{ax}\text{-}^{18}O\text{-}F_{ax})$ bands.

Table 1: Calculated and observed vibrational wavenumbers ν of $[OF_3]^-$ (CCSD(T)/aug-cc-pVTZ). Wavenumbers are given in cm^{-1}, IR intensities in km/mol.

vibrational mode	calc. harmonic ν (IR intensity)	calc. anharmonic[a] ν	exp. ν	exp. (calc.)[a] $\Delta\nu$ ($^{16/18}O$)
ν(O-F_{eq})	850.6 (48)	826.4	–	– (27.1)
ν_{as}(F_{ax}-O-F_{ax})	501.8 (816)	480.2	476.6	18.7 (18.0)
ν_{s}(F_{ax}-O-F_{ax})	406.0 (3)	396.8	–	– (0.5)
δ_{oop}	326.3 (5)	321.7	–	– (13.5)
δ_{as}	279.6 (203)	263.3	261.6	0.0 (−0.2)
δ_{s}	184.1 (3)	176.5	–	– (1.7)

[a] VCISDTQ

Due to residual $^{16}OF_2$ in the $^{18}OF_2$ sample and the similarity of the wavenumbers of $\delta(^{16}OF_2)$, $\delta(^{18}OF_2)$ and $\nu_{as}(F_{ax}$-^{18}O-$F_{ax})$, this band could only be analyzed by deconvolution of the spectrum (Figure 3).

The calculations predict only one other fundamental vibration within the range of the MCT detector (450–4000 cm^{-1}), namely ν(O-F_{eq}), which unfortunately overlaps with $\nu_{as}(OF_2)$ for both isotopologs. Even after irradiation ν(O-F_{eq}) could not be located in the difference spectra (Figure S4). This is not surprising as the concentration of $[OF_3]^-$, is fairly low compared to OF_2 even after 120 min of deposition and its band is predicted to be less than 6 % as intense as $\nu_{as}(F_{ax}$-O-$F_{ax})$. Also, the $\nu_{as}(OF_2)$ band changed its shape slightly upon irradiation and therefore complicated the detection of the ν(O-F_{eq}) signal. The δ_{as} vibration on the other hand, has a predicted intensity of ~25 % compared to $\nu_{as}(F_{ax}$-O-$F_{ax})$, making it in principle detectable, but the calculated wavenumber of 263.3 cm^{-1} is outside the MCT detector range. Motivated by these results, we measured far infrared (FIR) spectra employing a liquid-helium-cooled bolometer (180–700 cm^{-1}) for the heavier alkali metal fluorides KF, RbF and CsF. As expected from the calculations, the δ_{as} fundamental could be observed at 261.6 cm^{-1} without a detectable isotopic shift (Figure 4). The spectral signatures of the $[FOFF]^-$ isomer as well as the D_{3h} structure of $[OF_3]^-$ (a second-order transition state at the CCSD(T)/aug-cc-pVTZ level) are distinctly different (Table S1) and do not match with the observed bands, confirming the T-shape structure of the $[OF_3]^-$ species. Also, the calculated vibrational frequencies of the C_s-symmetric $[OF_3]^-$ $^3A''$ state differs clearly from the experimental data and is calculated to be higher in energy by 83 kJ/mol (Figure S1 and Table S1).

Note that no corresponding bands could be detected by conducting similar experiments in argon, which indicates that $[OF_3]^-$ might not be formed in a more strongly interacting environment (Table S5 and Figure S7), in agreement with previous observations for $[F_5]^-$.[16]

As mentioned above, the C_{2v}-symmetric T-shape structure of $[OF_3]^-$ is consistent with the prediction of the VSEPR model, in which the lone pairs are more space-demanding than the ligands (Figure 1). This argument was also used to explain smaller bond angles than in the ideal parent polyhedron. The textbook example ClF_3, which is valence isoelectronic to $[OF_3]^-$, shows an F_{eq}-Cl-F_{ax} angle of

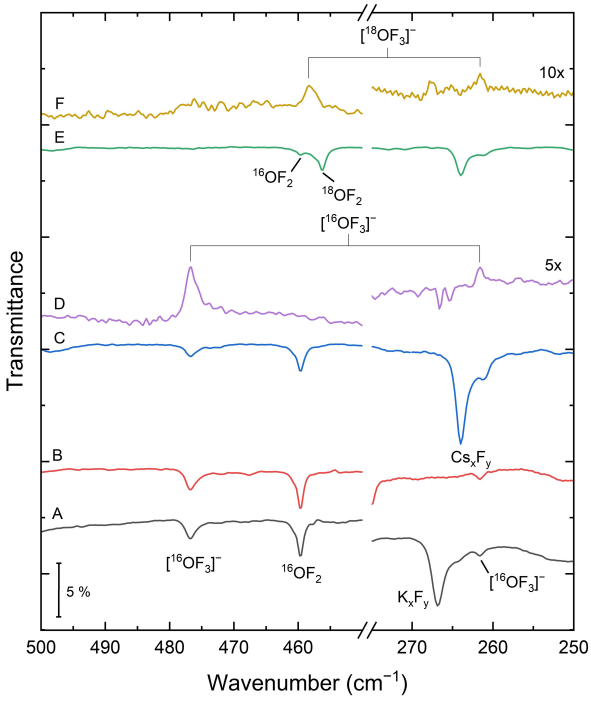

Figure 4. Far-IR spectra of the reaction products after co-deposition of 0.1 % OF_2 in Ne with laser ablated metal fluorides for 120 min before and after subsequent irradiation. Spectra D and F are difference spectra. A: KF. B: RbF. C: CsF. D: After irradiation with 275 nm for 10 min. E: Experiment with CsF and $^{18}OF_2$. F: After irradiation with 275 nm for 10 min.

87°.[17] Interestingly, the molecular structure of $[OF_3]^-$ shows a deviation in the opposite direction. The pseudo-axial fluorine atoms F_{ax} are bent away from the pseudo-equatorial fluorine atom F_{eq} by 98.1° at the CCSD(T)/aug-cc-pVTZ level, which has also been reported for higher chalcogen halides that are valence isoelectronic to $[OF_3]^-$. This abnormal behavior has been attributed to a greater demand for space by the equatorial halide ligand which accumulates some negative charge.[18] A systematic study of $[OF_3]^-$ homologs reveals that the X_{eq}-Y-Z_{ax} angle increases with the size of the ligands (X = H, F, Cl; Z = F, Cl) and decreases with the size of the central atom and its lone pairs (Y = O, S) (Figure S8). The influence of ligand-ligand repulsion on molecular geometry is described in the ligand close packing

model, which in conjunction with VSEPR has been shown to give better predictions.[17] The qualitatively wrong D_{3h}-symmetric structure predicted previously at the MP2/6-311+G(3df) level can be attributed to an insufficient basis set size, as concluded from tests with different combinations of methods and basis sets (Table S6).

To further characterize the potential energy hypersurface and interconversion between equivalent isomers, a relaxed energy surface scan along the F–O–F bond angles was conducted at the CCSD(T)/aug-cc-pVTZ level (Figure 5a). Three equivalent minimum structures are connected by first-order saddle points of C_{2v} symmetry with a relative energy of $E_0 = 13.6$ kJ/mol (16.88 kJ/mol before harmonic zero-point correction). The interconversion of the minima via the transition states proceed through a C_s-symmetric structure as shown by an intrinsic reaction coordinate (IRC) calculation (Figure 5a). These transition states are structurally and energetically very close to the D_{3h}-symmetric second-order saddle point at 13.3 kJ/mol (16.91 kJ/mol before harmonic zero-point correction) above the minimum structure (Figure S1).

The natural local molecular orbitals (NLMO) show that there are two different types of chemical bonding present in the molecule (Figure 5b). First, the O-F_{eq} bond is well described as a 2c–2e interaction. Analysis of the topology of the electron density and other parameters at the bond critical point (BCP) as well as the bond lengths indicate that

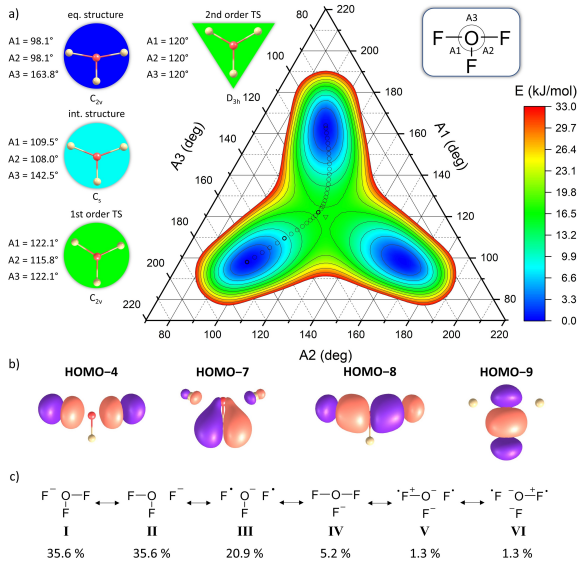

Figure 5. a) Potential energy surface of $[OF_3]^-$ along the F–O–F bond angles calculated at the CCSD(T)/aug-cc-pVTZ level. The data from the IRC scan are marked as black circles with bold circles indicating the position of the shown structures, whereas the 2nd order saddle point is marked as an inverted triangle. Note that the energies depicted here do not include zero-point vibrational energy. b) NLMOs of $[OF_3]^-$, that contribute to the O–F bonds. HOMO−4 and −8 are the non-bonding and bonding orbitals, respectively, which constitute a 3c–4e bond in the Rundle-Pimentel model. HOMO−7 is an in-plane p orbital of F_{eq} that mixes with the anti-bonding orbital. HOMO−9 represents the 2c–2e bond between O and F_{eq}. c) Resonance structures of $[OF_3]^-$ and their weights according to natural resonance theory (NRT).

this bond is not much different from those in OF_2 (Table S7). The second interaction is represented by two doubly occupied NLMOs that extend over the central oxygen atom and the two axial fluorine atoms and is therefore assigned to a 3c–4e interaction. They can be designated as the bonding and non-bonding orbital according to the Rundle-Pimentel model. Also, the doubly occupied p orbital of F_{eq}, that lies in the molecular plane, mixes with the antibonding orbital, which destabilizes the bond. In addition to the two bonding electron pairs, two lone pairs are located at the oxygen atom (Figure S9). This sets it apart from the long-known triethyloxonium cation $[(C_2H_5)_3O]^+$, that has a pyramidal structure in the solid state, which was attributed to the presence of one lone pair and three ligands in the coordination sphere of the oxygen.[19]

Evidently, the F_{ax}-O-F_{ax} interaction differs from the O–F bond in OF_2, which can be also seen by analysis of the electron density at the BCPs. The parameters show a close resemblance to the ones obtained for $[F_3]^-$, highlighting the similar character of these two systems (Table S7). This type of bonding is referred to as charge-shift bonding, which is typical for bonds in hypervalent molecules and bonds between elements with high electronegativity and a high number of lone pairs.[20]

The similarities between $[OF_3]^-$ and $[F_3]^-$ are also apparent from their resonance structures (Figures 5c and S10). The electronic structure is dominated by the ionic forms I and II, that are typically used to explain electron distribution in hypervalent compounds and represent the interaction of OF_2 with F^-.[7] What is remarkable is that the previously termed non-bonding structure III has a significant weight, which has been argued to be a major component of the stability of $[F_3]^-$ according to VB calculations.[5b] As this resonance structure represents the combination of $F^\bullet$ with $[OF_2]^{\bullet-}$, the stability of the latter is an important contributor to the stability of $[OF_3]^-$, which is also a necessary condition in the recoupled-pair bonding formalism for the formation of stable hypervalent compounds. The dissociation energy of $[OF_2]^{\bullet-}$ either towards $^\bullet OF$ and F^- or $F^\bullet$ and $[OF]^-$ for various computational methods is reasonably high (Table S12) and comparable to other 2c–3e systems, that are known to form stable hypervalent compounds.[6a] Looking at the frontier orbitals of $[OF_2]^{\bullet-}$ (Tables S8–S12 and Figure S11) also hints towards the resulting (electronic) structure obtained for $[OF_3]^-$, that is formally generated by addition of $F^\bullet$. The free $[OF_2]^{\bullet-}$ ion could not be detected, but the ion pairs MOF_2 (M = Na–Cs) (Table S13 and Figures S12–17).

In summary, we were able to extend the number of hypervalent second-row species by synthesizing the long-sought $[OF_3]^-$ through the reaction of OF_2 with F^- from laser-ablation of alkali metal fluorides, isolated in Ne under cryogenic conditions. The identity of the product was verified by MIR and FIR spectroscopy in isotopic-labeling experiments in combination with high-level ab-initio quantum-chemical calculations. The molecule adopts a C_{2v}-symmetric T-shape molecular structure, with the bonding best described as a 3c–4e interaction for the F_{ax}-O-F_{ax} bond and as a 2c–2e interaction for the O-F_{eq} bond. All bonds

have charge-shift character as shown by QTAIM and NRT analysis.

Supporting Information

The authors have cited additional references within the Supporting Information.[21–30]

Acknowledgements

We thank Dr. Carsten Müller, Dr. Simon Steinhauer, Dr. habil. Helmut Beckers, Xiya Xia, and Mei Wen for helpful discussions. We thank Anna Schröder for designing the Figure for the table of contents. We thank the HPC-service of the FUB-IT, Freie Universität Berlin, for the provision of computing resources. Also, we thank the Deutsche Forschungsgemeinschaft (DFG, German Research Foundation)—CRC 1349 "Fluorine-Specific Interactions"; Proj-ID 387284271—for funding. Open Access funding enabled and organized by Projekt DEAL.

Conflict of Interest

The authors declare no conflict of interest.

Data Availability Statement

The data that support the findings of this study are available from the corresponding author upon reasonable request.

Keywords: Hypervalent compounds · Matrix isolation spectroscopy · Oxygen · Fluorine · Main Group Fluorides

[1] a) I. Langmuir, *Science* **1921**, *54*, 59–67; b) G. N. Lewis, *J. Am. Chem. Soc.* **1916**, *38*, 762–785.
[2] J. I. Musher, *Angew. Chem. Int. Ed.* **1969**, *8*, 54–68.
[3] a) R. J. Hach, R. E. Rundle, *J. Am. Chem. Soc.* **1951**, *73*, 4321–4324; b) G. C. Pimentel, *J. Chem. Phys.* **1951**, *19*, 446–448.
[4] V. P. Oliveira, E. Kraka, F. B. C. Machado, *Inorg. Chem.* **2019**, *58*, 14777–14789.
[5] a) M. L. Munzarová, R. Hoffmann, *J. Am. Chem. Soc.* **2002**, *124*, 4787–4795; b) B. Braïda, P. C. Hiberty, *J. Am. Chem. Soc.* **2004**, *126*, 14890–14898; c) B. Braïda, P. C. Hiberty, *Nat. Chem.* **2013**, *5*, 417–422.
[6] a) T. H. Dunning, Jr., D. E. Woon, J. Leiding, L. Chen, *Acc. Chem. Res.* **2013**, *46*, 359–368; b) D. E. Woon, T. H. Dunning, Jr., *J. Phys. Chem. A* **2009**, *113*, 7915–7926.
[7] B. Braïda, P. C. Hiberty, *J. Phys. Chem. A* **2008**, *112*, 13045–13052.
[8] a) M. C. Durrant, *Chem. Sci.* **2015**, *6*, 6614–6623; b) B. Braida, T. Ribeyre, P. C. Hiberty, *Chem. Eur. J.* **2014**, *20*, 9643–9649.
[9] W. Kutzelnigg, *Angew. Chem. Int. Ed.* **1984**, *23*, 272–295.
[10] a) F. A. Redeker, H. Beckers, S. Riedel, *RSC Adv.* **2015**, *5*, 106568–106573; b) S. Riedel, T. Köchner, X. Wang, L. Andrews, *Inorg. Chem.* **2010**, *49*, 7156–7164.
[11] a) A. A. Tuinman, A. A. Gakh, R. J. Hinde, R. N. Compton, *J. Am. Chem. Soc.* **1999**, *121*, 8397–8398; b) A. Artau, K. E. Nizzi, B. T. Hill, L. S. Sunderlin, P. G. Wenthold, *J. Am. Chem. Soc.* **2000**, *122*, 10667–10670.
[12] K. Sonnenberg, L. Mann, F. A. Redeker, B. Schmidt, S. Riedel, *Angew. Chem. Int. Ed.* **2020**, *59*, 5464–5493.
[13] a) I. Anusiewicz, S. Freza, C. Sikorska, P. Skurski, *Chem. Phys. Lett.* **2010**, *493*, 234–237; b) I. V. Getmanskii, R. M. Minyaev, V. I. Minkin, *Russ. Chem. Bull.* **2012**, *61*, 2036–2048; c) D. J. Grant, T.-H. Wang, M. Vasiliu, D. A. Dixon, K. O. Christe, *Inorg. Chem.* **2011**, *50*, 1914–1925.
[14] F. A. Redeker, A. Kropman, C. Müller, S. E. Zewge, H. Beckers, B. Paulus, S. Riedel, *J. Fluorine Chem.* **2018**, *216*, 81–88.
[15] R. G. Pearson, *J. Am. Chem. Soc.* **1963**, *85*, 3533–3539.
[16] T. Vent–Schmidt, F. Brosi, J. Metzger, T. Schlöder, X. Wang, L. Andrews, C. Müller, H. Beckers, S. Riedel, *Angew. Chem. Int. Ed.* **2015**, *54*, 8279–8283.
[17] R. J. Gillespie, E. A. Robinson, *Chem. Soc. Rev.* **2005**, *34*, 396–407.
[18] K. C. Lobring, C. Hao, J. K. Forbes, M. R. J. Ivanov, S. M. Bachrach, L. S. Sunderlin, *J. Phys. Chem. A* **2003**, *107*, 11153–11160.
[19] M. I. Watkins, W. M. Ip, G. A. Olah, R. Bau, *J. Am. Chem. Soc.* **1982**, *104*, 2365–2372.
[20] S. Shaik, D. Danovich, J. M. Galbraith, B. Braïda, W. Wu, P. C. Hiberty, *Angew. Chem. Int. Ed.* **2020**, *59*, 984–1001.
[21] A. H. Borning, K. E. Pullen, *Inorg. Chem.* **1969**, *8*, 1791–1791.
[22] a) A. D. Becke, *J. Chem. Phys.* **1993**, *98*, 5648–5652; b) C. Lee, W. Yang, R. G. Parr, *Phys. Rev. B* **1988**, *37*, 785; c) P. J. Stephens, F. J. Devlin, C. F. Chabalowski, M. J. Frisch, *J. Phys. Chem.* **1994**, *98*, 11623–11627; d) S. H. Vosko, L. Wilk, M. Nusair, *Can. J. Phys.* **1980**, *58*, 1200–1211.
[23] a) S. Grimme, J. Antony, S. Ehrlich, H. Krieg, *J. Chem. Phys.* **2010**, *132*, 154104; b) S. Grimme, S. Ehrlich, L. Goerigk, *J. Comput. Chem.* **2011**, *32*, 1456–1465; c) D. G. A. Smith, L. A. Burns, K. Patkowski, C. D. Sherrill, *J. Phys. Chem. Lett.* **2016**, *7*, 2197–2203.
[24] M. J. Frisch, G. W. Trucks, H. B. Schlegel, G. E. Scuseria, M. A. Robb, J. R. Cheeseman, G. Scalmani, V. Barone, G. A. Petersson, H. Nakatsuji, X. Li, M. Caricato, A. V. Marenich, J. Bloino, B. G. Janesko, R. Gomperts, B. Mennucci, H. P. Hratchian, J. V. Ortiz, A. F. Izmaylov, J. L. Sonnenberg, Williams, F. Ding, F. Lipparini, F. Egidi, J. Goings, B. Peng, A. Petrone, T. Henderson, D. Ranasinghe, V. G. Zakrzewski, J. Gao, N. Rega, G. Zheng, W. Liang, M. Hada, M. Ehara, K. Toyota, R. Fukuda, J. Hasegawa, M. Ishida, T. Nakajima, Y. Honda, O. Kitao, H. Nakai, T. Vreven, K. Throssell, J. A. Montgomery Jr., J. E. Peralta, F. Ogliaro, M. J. Bearpark, J. J. Heyd, E. N. Brothers, K. N. Kudin, V. N. Staroverov, T. A. Keith, R. Kobayashi, J. Normand, K. Raghavachari, A. P. Rendell, J. C. Burant, S. S. Iyengar, J. Tomasi, M. Cossi, J. M. Millam, M. Klene, C. Adamo, R. Cammi, J. W. Ochterski, R. L. Martin, K. Morokuma, O. Farkas, J. B. Foresman, D. J. Fox, Wallingford, CT, **2016**.
[25] a) H. J. Werner, P. J. Knowles, G. Knizia, F. R. Manby, M. Schütz, *WIREs Comput. Mol. Sci.* **2012**, *2*, 242–253; b) H.-J. Werner, P. J. Knowles, F. R. Manby, J. A. Black, K. Doll, A. Heßelmann, D. Kats, A. Köhn, T. Korona, D. A. Kreplin, Q. Ma, T. F. Miller, III, A. Mitrushchenkov, K. A. Peterson, I. Polyak, G. Rauhut, M. Sibaev, *J. Chem. Phys.* **2020**, *152*, 144107; c) H. J. Werner, P. J. Knowles, P. Celani, W. Györffy, A. Hesselmann, D. Kats, G. Knizia, A. Köhn, T. Korona, D. Kreplin, R. Lindh, Q. Ma, F. R. Manby, A. Mitrushenkov, G. Rauhut, M. Schütz, K. R. Shamasundar, T. B. Adler, R. D. Amos, S. J. Bennie, A. Bernhardsson, A. Berning, J. A. Black, P. J. Bygrave, R. Cimiraglia, D. L. Cooper, D. Coughtrie,

M. J. O. Deegan, A. J. Dobbyn, K. Doll, M. Dornbach, F. Eckert, S. Erfort, E. Goll, C. Hampel, G. Hetzer, J. G. Hill, M. Hodges, T. Hrenar, G. Jansen, C. Köppl, C. Kollmar, S. J. R. Lee, Y. Liu, A. W. Lloyd, R. A. Mata, A. J. May, B. Mussard, S. J. McNicholas, W. Meyer, T. F. Miller, M. E. Mura, A. Nicklass, D. P. O'Neill, P. Palmieri, D. Peng, K. A. Peterson, K. Pflüger, R. Pitzer, I. Polyak, M. Reiher, J. O. Richardson, J. B. Robinson, B. Schröder, M. Schwilk, T. Shiozaki, M. Sibaev, H. Stoll, A. J. Stone, R. Tarroni, T. Thorsteinsson, J. Toulouse, M. Wang, M. Welborn, B. Ziegler, **2021**.

[26] E. D. Glendening, J. K. Badenhoop, A. E. Reed, J. E. Carpenter, J. A. Bohmann, C. M. Morales, P. Karafiloglou, C. R. Landis, F. Weinhold, Theoretical Chemistry Institute, University of Wisconsin, Madison, **2018**.

[27] T. Lu, F. Chen, *J. Comput. Chem.* **2012**, *33*, 580–592.

[28] G. Herzberg, *Molecular Spectra and Molecular Structure—III. Electronic Spectra and Electronic Structure of Polyatomic Molecules*, Van Nostrand Reinhold, New York, **1966**.

[29] a) R. F. W. Bader, *Atoms in molecules, Vol. 22*, Clarendon Press, Oxford, **1994**; b) H. Keil, K. Sonnenberg, C. Müller, R. Herbst-Irmer, H. Beckers, S. Riedel, D. Stalke, *Angew. Chem. Int. Ed.* **2021**, *60*, 2569–2573; c) E. Espinosa, I. Alkorta, J. Elguero, E. Molins, *J. Chem. Phys.* **2002**, *117*, 5529–5542; d) S. Shaik, D. Danovich, J. M. Galbraith, B. Braïda, W. Wu, P. C. Hiberty, *Angew. Chem. Int. Ed.* **2020**, *59*, 984–1001.

[30] a) A. D. Becke, K. E. Edgecombe, *J. Chem. Phys.* **1990**, *92*, 5397–5403; b) B. Silvi, A. Savin, *Nature* **1994**, *371*, 683–686.

Manuscript received: July 22, 2024
Accepted manuscript online: October 15, 2024
Version of record online: November 16, 2024